Unveiling the interplay of Mollow physics and perturbed free induction decay by nonlinear optical signals of a dynamically driven two-level system

Jan M. Kaspari [1], Thomas K. Bracht [1], Katarina Boos [2], Sang Kyu Kim [2], Friedrich Sbresny [2], Kai Müller [2], and Doris E. Reiter [1]

[1]*Condensed Matter Theory, Department of Physics, TU Dortmund, 44221 Dortmund, Germany*
[2]*Walter Schottky Institut, TUM School of Computation, Information and Technology, and MCQST,
Technische Universität München, 85748 Garching, Germany*

Nonlinear optical signals in optically driven quantum systems can reveal coherences and thereby open up the possibility for manipulation of quantum states. While the limiting cases of ultrafast and continuous-wave excitation have been extensively studied, the time dynamics of finite pulses bear interesting phenomena. In this paper, we explore the nonlinear optical probe signals of a two-level system excited with a laser pulse of finite duration. In addition to the prominent Mollow peaks, the probe spectra feature several smaller peaks for certain time delays. Similar features have been recently observed for resonance fluorescence signals [K. Boos *et al.*, Phys. Rev. Lett. **132**, 053602 (2024)]. We discuss that the emergent phenomena can be explained by a combination of Mollow triplet physics and perturbed free induction decay effects, providing an insightful understanding of the underlying physics.

I. INTRODUCTION

Linear and nonlinear optical signals are powerful tools to investigate quantum emitters in order to achieve new ways of manipulation for quantum technologies. In such signals, the quantum emitter is excited by a single or a set of laser pulses and the system's response is monitored with different outputs depending on the signal of interest.

One class of optical signals is resonance fluorescence, i.e., the emission of a resonantly, coherently driven system [1,2]. A prominent example of coherent physics in resonance fluorescence is the Mollow triplet occurring for driving with a continuous-wave (cw) excitation [3]. The Mollow triplet has been measured for quantum emitters such as semiconductor quantum dots [4–6] or other artificial two-level systems such as superconducting circuits [7]. Moving from cw excitation to finite pulses, a more complex spectrum emerges in the resonance fluorescence [8–12]. For finite Gaussian pulses, additional peaks appear between the central and outer Mollow lines. Measuring time-dependent dressed states poses a high demand on the experimental setup and measurement fidelity, especially for quantum emitters working in the optical regime. Therefore, the full emission spectrum of a quantum dot, showing multiple side peaks, was only experimentally detected recently [13,14], coined as dynamical Mollow triplet.

Another class of optical signals is the spectra gained in coherent control experiments [15]. In such experiments, a pump pulse creates a coherence in the system, which is probed by following pulses. In most cases, the exciting laser pulses are much shorter than the timescales of the system. In the simplest case, two pulses are employed in pump-probe spectroscopy [16–19], but also four- or six-wave-mixing spectroscopy techniques are commonly used [20–23]. Interestingly, if the order of pulses is inverted, i.e., the probe pulse comes before the pump pulse, a perturbed free induction decay occurs [24–33]. In the spectra, this manifests as fringes in addition to the main peak.

Motivated by recent experimental findings on the dynamical Mollow spectrum [13,14], in this paper, we study the emergence of the observed features by simulating the optical signals of a finite excitation pulse within a pump-probe setup. Choosing a pump-probe configuration over resonance fluorescence has the advantage of access to the dynamics of the system. For this, we extend the methods presented in Refs. [34,35], where the case of a cw pump pulse was studied, to finite pulses. Due to the knowledge of the time-resolved dynamics, we can unveil the interplay of Mollow triplet physics and perturbed free induced decay in the probe spectra. Comparing our findings in the probe spectra to the spectra measured in resonance fluorescence [13], we find a good agreement between the main features as the physics behind both signals is the same.

II. THEORETICAL BACKGROUND

To model the optical signals, we consider a two-level system, which is a common model for quantum emitters such as quantum dots. The two levels are the ground state $|g\rangle$ and the exciton state $|x\rangle$ separated by the energy difference E_x. The coupling to an external driving light field is described
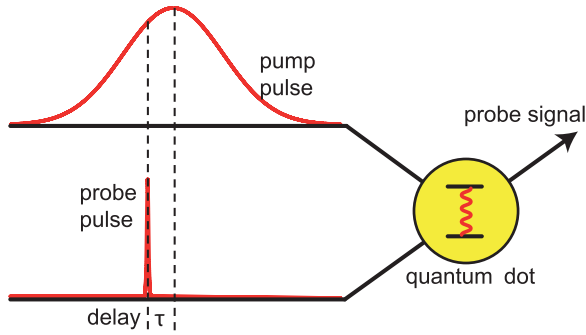
FIG. 1. Scheme of a pump-probe setup as described in detail in the text.

semiclassically in the dipole and rotating wave approximation. The light field energy $\hbar\omega_L$ with the laser frequency ω_L is assumed to be resonant to the transition between the two states. Under these conditions, the Hamiltonian

$$H = -\frac{\hbar}{2}[\tilde{\Omega}^*(t)\,|g\rangle\,\langle x| + \tilde{\Omega}(t)\,|x\rangle\,\langle g|] \tag{1}$$

describes the carrier light interaction via the light field $\tilde{\Omega}(t) = \Omega(t)\exp(-i\omega_L t)$, where $\Omega(t)$ denotes the complex, temporal envelope of the field. By transforming into the rotating frame, this Hamiltonian can be rewritten as

$$H = -\frac{\hbar}{2}[\Omega^*(t)\,|g\rangle\,\langle x| + \Omega(t)\,|x\rangle\,\langle g|]. \tag{2}$$

Considering a pump-probe setup, we are interested in the probe signals under different pulse shapes of the pump laser. A schematic drawing of such a setup is shown in Fig. 1. In these kinds of experiments, a pump pulse is used to excite the system, i.e., inducing a dynamic change. After a time delay τ, with respect to the pump pulse, a second pulse is used to probe the response of the system. While the pump pulse can be strong, e.g., it can cause a complete population inversion, the ultrashort probe pulse is so weak that it hardly influences the dynamics of the system.

The envelope of the complete light field is composed of the pump pulse Ω_{pump} and the probe pulse Ω_{probe},

$$\Omega(t) = \Omega_{\text{pump}}(t) + \Omega_{\text{probe}}(t - \tau)e^{i\Phi}. \tag{3}$$

We assume a phase factor $e^{i\Phi}$ between the pump and probe pulse. Using the Hamiltonian with the two light fields, we set up the equations of motion and solve these by numerical integration.

To calculate the probe polarization, following Ref. [32], we expand the optical polarization $\boldsymbol{P}(t, \tau, \Phi)$ in a Fourier series with respect to the phase factor,

$$\boldsymbol{P}(t, \tau, \Phi) = \sum_n \boldsymbol{P}_n(t, \tau)e^{-in\Phi}, \tag{4}$$

and perform a phase selection. The desired probe polarization is calculated by the Fourier coefficient,

$$\boldsymbol{P}_n(t, \tau) = \frac{1}{2\pi}\int_0^{2\pi} d\Phi\,\boldsymbol{P}(t, \tau, \Phi)e^{in\Phi}, \tag{5}$$

for $n = 1$. The absorption spectrum is described based on the absorption coefficient, which can be determined by

calculating the imaginary part of the Fourier transformation of the probe polarization [34],

$$\alpha(\omega) = \text{Im}\{\mathcal{F}[P_1(t, \tau) \cdot e^{-\Gamma t}]\}. \tag{6}$$

When we refer to absorption in the spectrum, this correlates to positive absorption coefficients, while negative values indicate a gain or emission. Furthermore, we introduce a damping to the polarization with the damping coefficient $\Gamma = 0.139\ \text{ps}^{-1}$. While this damping can be used to describe a loss of optical polarization in the system due to the interaction with the environment, in this work it is purposely chosen in such a way that it highlights the underlying physical effects. As such, the value of Γ is enhanced compared to what is found for typical decoherence effects to help visualize the physics behind the findings.

III. RESULTS

The results are structured as follows: We begin by briefly summarizing the known limiting cases of the pump pulse being either a cw pulse switched on instantaneously or an ultrashort pulse in the δ-pulse limit. Understanding these cases will set the stage to discuss the probe spectra for finite pulses. For this, we start by examining rectangular pulses and then gradually transition to Gaussian pulses by softening the pulse edges. To connect our calculations with real-world numbers, we consider typical timescales of quantum dot dynamics [13], which gives a typical timescale of picoseconds. We conclude by comparing our findings for the probe spectra with measurements in resonance fluorescence from Ref. [13].

In all cases, we consider an ultrafast probe pulse, which, in the numerical calculations, is given by a Gaussian pulse with the envelope

$$\Omega_{\text{probe}}(t) = \frac{\alpha_{\text{probe}}}{\sqrt{2\pi\sigma_{\text{probe}}^2}}\exp\left(\frac{-(t - \tau)^2}{2\sigma_{\text{probe}}^2}\right). \tag{7}$$

The pulse area of the probe pulse is set to be very weak with $\alpha_{\text{probe}} = 0.02\pi$ and, to have an ultrashort pulse, we set the pulse width to $\sigma_{\text{probe}} = 10\ \text{fs}$. The delay τ of the probe pulse defines the time difference between the pump and probe pulse, as discussed below for the different pump pulses.

A. Limiting cases

The first limiting case is the one of cw excitation. Thus, for the pump pulse, we consider a constant pulse with pulse strength Ω_{cw} switched on instantaneously,

$$\Omega_{\text{pump}}(t) = \Omega_{\text{cw}}\,\Theta(t - NT_R),$$

where Θ is the Heaviside function. We set the starting point of the pulse to $-N$ oscillation periods, such that the reference point for the probe pulse is the Nth maximum of oscillation. This leads to Rabi oscillations with the period $T_R = 2\pi/\Omega_{\text{cw}}$.

We set $\hbar\Omega_{\text{cw}} = 2\ \text{meV}$, i.e., $\Omega_{\text{cw}} = 3.039\ \text{ps}^{-1}$ and $T_R = 2.066\ \text{ps}$. Initially, the system is in its ground state and we choose $N = 250$. As we work in a rotating frame, the energy $\hbar\omega = 0$ refers to the transition energy of the system.

The resulting probe spectra for different delays τ are shown in Fig. 2. They are all normalized to the middle peak for
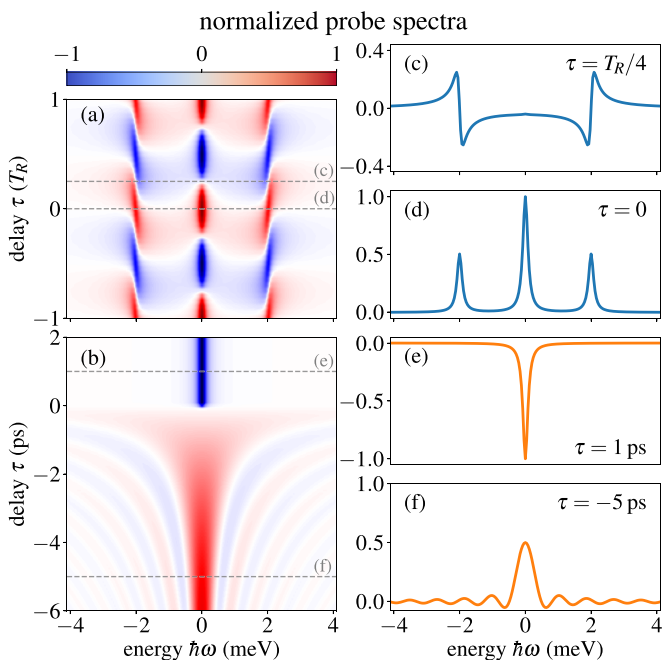
FIG. 2. Color plot of the normalized probe spectrum (a) under cw excitation switched on instantaneously as a function of delay τ for two periods from $-T_R$ (-2.06 ps) to T_R (2.06 ps) and (b) for δ-pulse excitation at $\tau = 0$ as a function of τ. Cuts showing probe spectra for the cw pump at (c) $\tau = T_R/4$ and (d) $\tau = 0$ and for ultrafast excitation at (e) $\tau = 1$ ps and (f) $\tau = -5$ ps.

$\tau = 0$. Due to the periodicity of the Rabi oscillations for a cw laser, the spectra are the same for $\tau \rightarrow \tau + nT_R$, with $n \in \mathcal{N}$. Theses spectra exhibit three distinct peaks at $\hbar\omega = 0$ and $\hbar\omega = \pm\hbar\Omega_R$, as known from the Mollow triplet. The amplitude variations in these peaks reflect the dynamics of the two-level system. When the peaks have a positive amplitude, the system is in the ground state, while negative amplitudes correspond to the system being in the excited state. For the time delays $\tau = T_R/4$ and $\tau = 3T_R/4$, both states are half occupied, resulting in the disappearance of the middle peak, with gain and absorption balancing each other out. Exemplary cuts of the spectra are shown in Fig. 2(c) for $T_R/4$ and in Fig. 2(d) for $\tau = 0$. This system dynamics, also including phonons and detuning, is discussed in detail in Refs. [34,35].

In the second limiting case, we consider an ultrafast pump pulse, such that there is no overlap between the pump and probe pulse. The resulting spectra are shown in Fig. 2(b). In the simulations, we approximate the δ pulses with ultrashort Gaussian pulses,

$$\Omega_{\text{pump}}(t) = \frac{\alpha_{\text{uf}}}{\sqrt{2\pi\sigma_{\text{uf}}^2}} e^{-\frac{t^2}{2\sigma_{\text{uf}}^2}} \xrightarrow{\sigma_{\text{uf}}^2 \rightarrow 0} \Omega_{\text{uf}}\delta(t). \quad (8)$$

Here, α_{uf} is the pulse area of the pulse, while in the numerics, we assume the pulse with $\sigma_{\text{uf}} = \sigma_{\text{probe}}$. The time delay refers to the difference between the two pulses.

In most cases, the order of pump and probe pulses is such that the pump pulse excites the system and the probe pulse arrives after the pump pulse. In our model, this corresponds to $\tau > 0$. Using a pulse area of π, the pump pulse inverts the

system and the excited state is fully occupied. Accordingly, for $\tau > 0$, we see a single negative peak at $\hbar\omega = 0$, corresponding to gain.

A distinctly different spectrum emerges for a negative time delay $\tau < 0$, where the probe pulse precedes the pump pulse. Instead of a single peak, we find a strong peak at $\hbar\omega = 0$, but with an amplitude smaller than one, next to a series of side peaks. An example is shown in Fig. 2(f). This is known as perturbed free induction decay [24–33]. With the probe pulse, the probe polarization starts to oscillate, but is then perturbed by the pump pulse. This results in a rectangular window for the probe polarization, which in the spectrum corresponds to a sinc function. The sinc function is now convoluted with the single peak, which describes the ripple structure observed in Figs. 2(b) and 2(f). We note that the occurrence of the ripple structure is strongly connected to the damping coefficient Γ used to calculate the polarization [cf. Eq. (5)]. If the probe polarization has decayed before the pump pulse sets in, the perturbed free induction decay is not observed.

B. Rectangular pump pulse

Now we want to expand the model to finite pulses. Coming from the limiting cases, the most simple case is a rectangular pulse of the form

$$\Omega_{\text{pump}}(t) = \Omega_{\text{rect}} \text{rect}\left(\frac{t}{NT_R}\right)$$

$$= \Omega_{\text{rect}} \Theta\left(t + \frac{1}{2}NT_R\right)\Theta\left(\frac{1}{2}NT_R - t\right).$$

We set $\hbar\Omega_{\text{rect}} = 2$ meV, i.e., $\Omega_{\text{rect}} = 3.039$ ps^{-1} and $T_R = 2.066$ ps. The total pump pulse duration is chosen such that $N = 20$ oscillation periods are included in the pulse, which results in a duration of $T_{\text{total}} = NT_R = 41.32$ ps. As a reference point for the time delay, we choose the center of the rectangular pulse.

The probe spectrum for a rectangular pulse as a function of time delay τ is depicted in Fig. 3. The pump pulse is centered at $t = 0$, and thus $\tau < -20.66$ ps refers to the probe pulse coming before the pump pulse and $\tau > 20.66$ ps after the pump pulse. We can discriminate four different regimes depending on the delay τ. We will explain the behavior using four selected spectra shown in Figs. 3(b)–3(e). The simplest case is shown in Fig. 3(b), where the probe pulse comes after the pump pulse. After the pump pulse, the system is in its ground state and, in agreement with the limiting case of a δ pulse, we see a single absorption line at 0 meV. The other limiting case of a cw excitation is achieved shortly after the pump pulse is switched on, e.g., at $\tau = -16.5$ ps, as shown in Fig. 3(d). Here, we again see three absorption lines as typical for a Mollow-type spectrum.

A quite different behavior occurs for probe pulses near the end of the pump pulse, as shown in Fig. 3(c). We observe an additional ripple structure modifying the Mollow triplet. In addition, the amplitude of the Mollow peaks is reduced. This is a consequence of effects similar to the perturbed free induction decay we already observed in the limiting case of ultrafast excitation with a pump pulse preceding the probe pulse. This results in the probe polarization being cut out
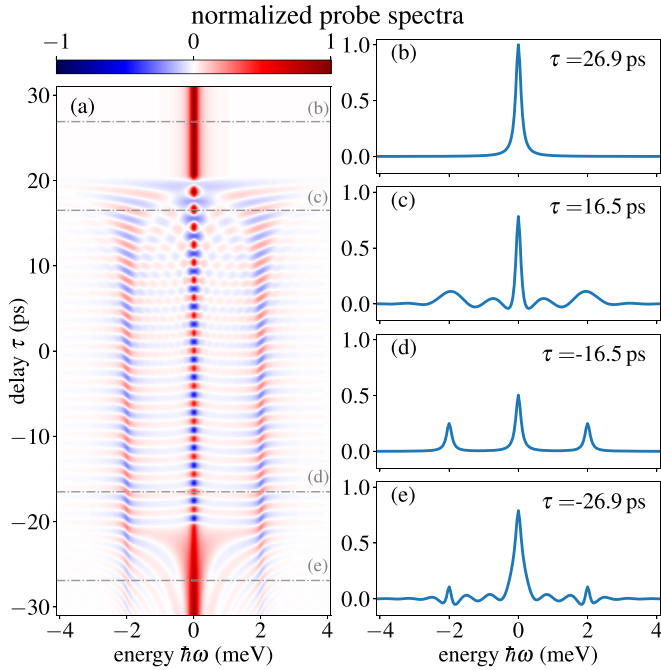
FIG. 3. (a) Color plot of the probe spectra for a rectangular pulse acting from -20.6 ps ($-10T_R$) to 20.6 ps ($10T_R$). Cuts through the color plot (highlighted with gray lines) show the probe spectra at (b) $\tau = 26.9$ ps, (c) $\tau = 16.5$ ps, (d) $\tau = -16.5$ ps, and (e) $\tau = -26.9$ ps.

with a rectangular window, defined by the probe pulse and the ending of the pump pulse. To illustrate this in more detail, we show the dynamics of the probe polarization together with the laser pulse sequence in Fig. 4. Note that in agreement with the rotating frame, we only show the modulation of the probe polarization. The probe pulse starts the probe dynamics at its onset at $t = 14.47$ ps and oscillates with the Rabi frequency during the action of the pump pulse. When the pump pulse ends, the probe polarization becomes constant again. The dashed curve in Fig. 4(b) shows the damped probe polarization used for the Fourier transform. This behavior yields a
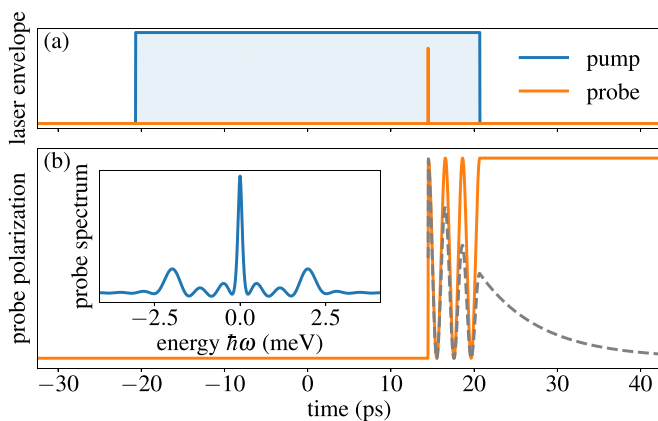

FIG. 4. (a) Laser envelopes of a rectangular pump pulse and an ultrashort probe pulse at $\tau = 14.47$ ps and corresponding (b) probe polarization (orange), damped probe polarization (gray), and probe spectrum (inset).
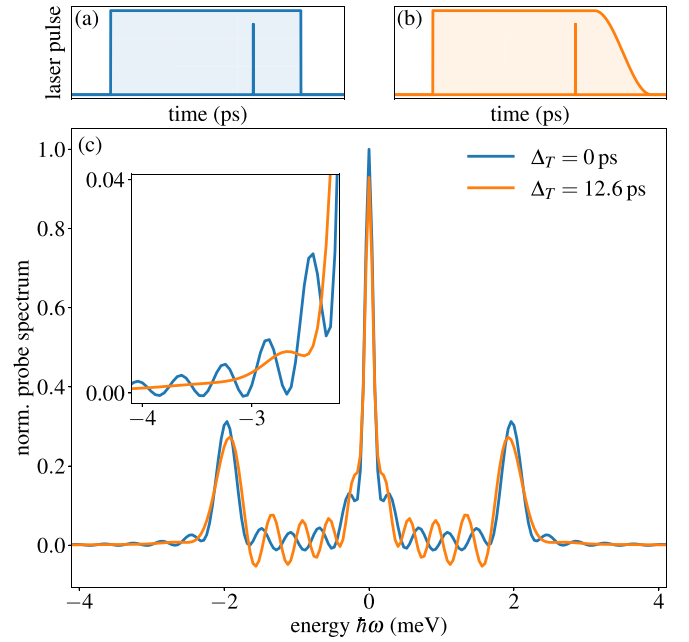

FIG. 5. Probe spectra for a rectangular pulse with a sharp edge (blue, $\Delta_T = 0$) and softened edge (orange, $\Delta_T = 12.6$ ps). Pulse sequences are shown above. In both cases, probing is performed 30.9 ps after the pump pulse has started.

spectrum that is a convolution of the Mollow triplet known from the cw limit with a sinc function.

In the last case [Fig. 3(e)], when the probe pulse acts before the pump pulse, i.e., $\tau < -20.66$ ps, there is no dynamical pattern and the central peak remains positive. As in the δ-pulse case, a ripple pattern occurs as expected for the perturbed free induction decay. Interestingly, the system already feels the onset of the cw pulse and a signature of the Mollow triplet is observed.

C. Smeared out laser pulse

In the next step, we analyze the influence of the pulse shape on the probe spectra during the pulse. We have seen that the switch-off is essential for the ripple pattern observed in addition to the Mollow triplet. Therefore, we soften the switch-off edge of the rectangular pulse, while maintaining a constant pulse area for the whole pulse. To achieve this, we divide our pulse into two separate parts, namely, the constant rectangular part and a softened edge,

$$\Omega_{\mathrm{pump}}(t) = \Omega_{\mathrm{rect}}(t) + \Omega_{\mathrm{off}}(t).$$

The softened edge is described by a $\cos^2$ function with a period of $2\Delta_T$ and a duration of Δ_T with the equation given in the Appendix. In the case of a sharp edge, the rectangular part is switched on at t_{on} and off at t_{off}. For a soft edge, both the pulse's position and its duration get adjusted in such a way that the pulse area over the whole pulse stays constant and the start of the pulse does not change. The time delay τ is chosen to coincide with a maximum of occupation shortly before the end of the pulse, i.e., to be in the same regime as in Fig. 3(c). Two examples for pump pulses are depicted in Figs. 5(a) and 5(b) for the cases $\Delta_T = 0$ ps and $\Delta_T = 12.6$ ps, respectively.
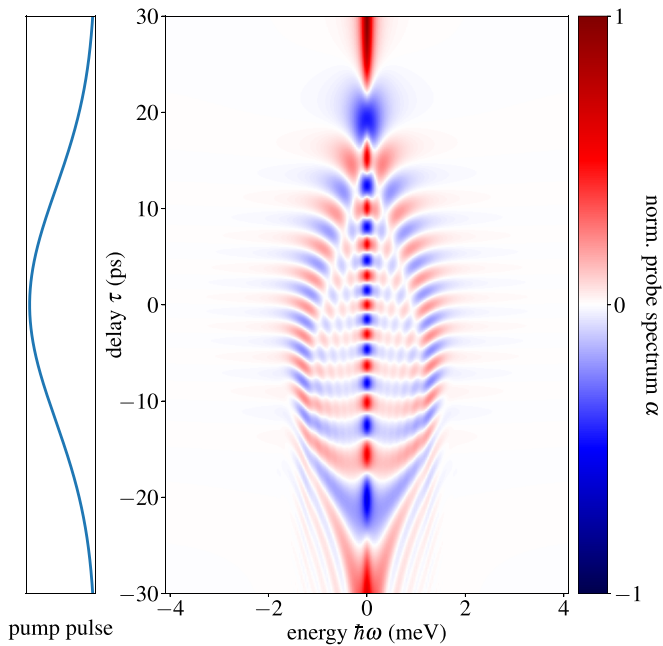
FIG. 6. Color plot of the probe spectra during the excitation with a Gaussian pulse for different time delays τ. The temporal profile of the pulse is depicted on the left side.

The resulting spectra for these two pulses are shown in Fig. 5(c). Both cases capture a similar structure: They both show a three-peak structure with additional minor peaks between them. Our focus lies on the behavior of these minor peaks. For the rectangular pulse, there are three peaks between each side and the central peak, all with similar strength. In the case of the softened edge, all peaks are slightly shifted to the main center peak. Additionally, their heights vary strongly from each other and increase the further away the associated peak is from the center. Another important difference is found outside of the outer Mollow peaks, which is highlighted in the inset of Fig. 5(c). We observe that peaks in this area, although already weak in the other studied cases, are damped away almost entirely.

D. Gaussian laser pulse

1. Pulse delay dependence

With these findings in mind, we want to investigate the spectrum of the probe signal of a Gaussian-shaped laser pulse, as used in many experiments,

$$\Omega_{\text{pump}}(t) = \frac{\alpha}{\sqrt{2\pi \sigma_P^2}} \exp\left(-\frac{t^2}{2\sigma_P^2}\right). \qquad (9)$$

The normalized probe spectra as a function of pulse delay are depicted in Fig. 6. For the Gaussian pulse, it is less obvious to define delays for which the probe pulse is clearly before or after the pulse. We speak of the onset of the pulse at roughly -20 ps, such that a delay of $\tau < -20$ ps corresponds to being before the pulse. Correspondingly, for delays of $\tau > 20$ ps, the pump pulse is mostly gone, so we speak of after the pulse. Before and after the pump pulse, the spectra are as expected. Of high interest is the behavior during the pulse for delays

$-20 < \tau < 20$ ps. For the Gaussian pulse, the instantaneous Rabi frequency changes continuously during the pulse. Accordingly, in the probe spectrum, we can identify two side peaks following the Gaussian shape of the pump pulse as a function of energy. The maximum splitting of the outer peaks is reached for $\tau = 0$ ps. In addition, the oscillation in the time delay due to the oscillating occupation is visible as well. At the same time, we notice the manifestation of an additional checkered pattern and a broadening of the peaks towards the end of the Gaussian pulse. All of these observations are consequences of the combined effects from Mollow triplet and perturbed free induction decay physics.

2. Pulse area dependence

Now that we understand the general concept of the underlying physics and especially the dependence of the spectrum on the pulse delay, we aim to match our findings with the observations in the resonance fluorescence experiments [13]. These experiments do not have access to the time-resolved dynamics during the pulse, but still the same ripple structure is observed in the spectra. Furthermore, increasing the pulse area results in the emergence of a stripe pattern. In order to match these findings, we investigate how the spectra depend on the pulse area. For that, we construct our pump pulse in such a way that a rectangular-shaped pulse part ensures that the system is always in the same state, i.e., the ground state, when the probe pulse hits the system at t_{probe}. Doing so eliminates the additional amplitude dynamics resulting from the system's state dynamics. Immediately after the probe pulse, the switch-off process begins, where the laser pulse is simulated by half a Gaussian pulse. The equations are given in the Appendix.

We compare our theoretical results for varying pump pulse areas in Fig. 7(a) with experimental data of the dynamical Mollow spectra in Fig. 7(b). Cuts of the spectra for a pulse area of 6π are displayed in Figs. 7(c) and 7(d). We obtain a central peak at $\hbar\omega = 0$ for all pulse areas. With increasing pulse area, the effective Rabi frequency increases approximately linearly, which is seen by the energy of the outermost side peaks. In between, we find the stripe pattern induced by the finite pulse length. For every pulse area increment of roughly 2π, an additional set of peaks inside the Mollow triplet appears. The same qualitative behavior is observed in the experimental data. The spectra for a given pulse area of 6π also match well with our simulations, as shown in Figs. 7(c) and 7(d). Note that due to our choice of Γ, we overestimate the magnitude of the side peaks, while for resonance fluorescence, due to the nature of the signal, the effects are smaller and a logarithmic scale was used. Besides the side peak, for $\hbar\omega > 0$, there are three signatures in both experiment and theory, the uttermost being the Mollow peak and two features from the perturbed free induction decay. On the lower energy $\hbar\omega < 0$ side, the theoretical spectrum again shows three peaks, while in the experimental data, a more uniform spectrum appears. Here, the interaction with acoustic phonons leads to the prominent phonon sidebands [36,37]. While the phonon relaxation can be described within a rate equation in the dressed states [34,35], phonon sidebands are a result of the polaron formation captured by non-Markovian approaches [38–41]. As the phonon sidebands are not the main focus of
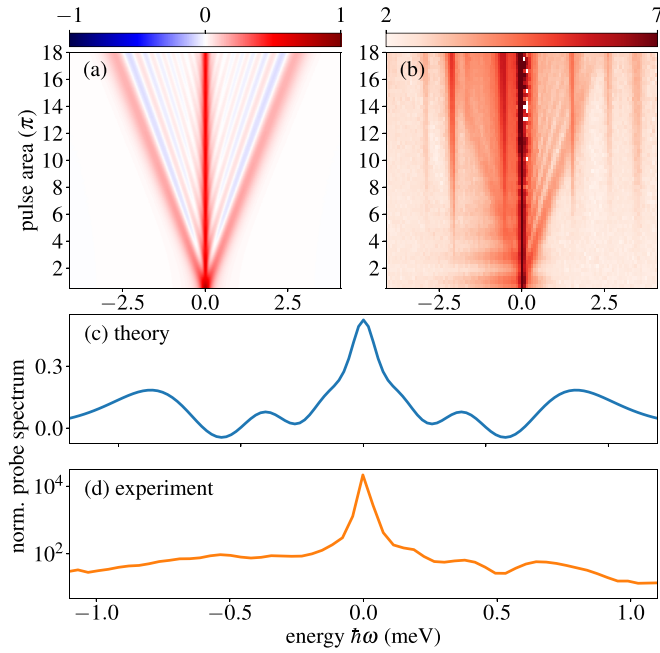
FIG. 7. Comparison of (a) theoretical and (b) experimental data for spectra with Gaussian-shaped pulses with a duration (FWHM) of 12 ps for different pulse areas. Cuts comparing the (c) theoretical and (d) experimental data for a pulse area of 6π. Here, the values for pulse areas and pulse duration of the theoretical pulses refer to after the probe pulse.

the work, we refrained from taking up the numerical effort to include these and describe well-established phenomena, but focused on the ripple structure visible in both pump-probe simulations and resonance fluorescence measurement.

IV. CONCLUSION

We have studied the time-resolved probe spectra of a dynamically driven two-level system. For the limiting cases of ultrashort laser pulses and continuous driving, we observed the well-established perturbed free induction decay and the Mollow triplet. We showed that for rectangular laser pulses, four distinctly different regimes can be identified—one where the spectral behavior is dominated by the Mollow triplet physics and one where the perturbed free induction decay determines the spectrum, and two regimes where the probe spectrum results from the interplay of both effects. In the latter regimes, alongside the Mollow triplet, an additional ripple pattern appears. Softening the switch-off process of these pulses and therefore changing their shape led not only to shifts of all peaks towards the center and changes in peak heights, but also to the disappearance of the spectrum outside of the outer Mollow peaks. All of the observed spectral features also

occur for Gaussian-shaped pulses and provide an insightful understanding of the formation and the underlying physics of the recently measured dynamical Mollow spectrum. In conclusion, we found that the probe spectra of nonlinear optical signals for finite pulses depend on both the pump pulse shape and duration, as well as the probe timing. They emerge as a consequence of the interplay between Mollow triplet physics and perturbed free induction decay.

APPENDIX: EQUATIONS FOR THE PULSES

For the pulse with softened edges, we use the following expressions:

$$\Omega_{\text{rect}}(t) = \Omega_{\text{rect}} \cdot \text{rect}\left(\frac{t + \Delta_T/4}{t_{\text{off}} - \Delta_T/2 - t_{\text{on}}}\right),$$

$$\Omega_{\text{off}}(t) = \Omega_{\text{rect}} \cdot \cos^2\left\{\frac{\pi}{2\Delta_T} \cdot [t - (t_{\text{off}} - \Delta_T/2)]\right\}.$$

For the pulse area dependence, the equation for the pulse reads

$$\Omega_{\text{pump}}(t, \alpha) = \begin{cases} \Omega_{\text{area}}(\alpha) \cdot \text{rect}\left(\frac{t - \frac{t_{\text{probe}} + t_{\text{on}}(\alpha)}{2}}{t_{\text{probe}} - t_{\text{on}}(\alpha)}\right), & t < t_{\text{probe}} \\ \frac{2\alpha}{\sqrt{2\pi\sigma_P^2}} e^{-\frac{(t - t_{\text{probe}})^2}{2\sigma_P^2}}, & t \geqslant t_{\text{probe}}, \end{cases}$$

where α refers to the pulse area after the probe pulse. A smooth transition between the two pulse parts and the desired selective state preparation at t_{probe}, removing additional amplitude dynamics in the probe spectrum, are both achieved by varying t_{on} and Ω_{area} for every value of α, such that they read

$$t_{\text{on}}(\alpha) = t_{\text{probe}} - \frac{\alpha_{\text{prep}}}{\Omega_{\text{area}}(\alpha)},$$

$$\Omega_{\text{area}}(\alpha) = \frac{\alpha}{\sqrt{2\pi\sigma_P^2}}.$$

The pulse area α_{prep} is chosen in such a way that the system is always in its ground state when its probed, i.e., $\alpha_{\text{prep}} = 2\pi$ in our calculations.

[1] H. J. Kimble and L. Mandel, Theory of resonance fluorescence, Phys. Rev. A **13**, 2123 (1976).

[2] A. Muller, E. B. Flagg, P. Bianucci, X. Y. Wang, D. G. Deppe, W. Ma, J. Zhang, G. J. Salamo, M. Xiao, and C. K. Shih, Resonance fluorescence from a coherently driven semiconductor quantum dot in a cavity, Phys. Rev. Lett. **99**, 187402 (2007).

[3] B. R. Mollow, Power spectrum of light scattered by two-level systems, Phys. Rev. **188**, 1969 (1969).

[4] A. Ulhaq, S. Weiler, S. M. Ulrich, R. Roßbach, M. Jetter, and P. Michler, Cascaded single-photon emission from the Mollow triplet sidebands of a quantum dot, Nat. Photon. **6**, 238 (2012).

[5] A. Ulhaq, S. Weiler, C. Roy, S. M. Ulrich, M. Jetter, S. Hughes, and P. Michler, Detuning-dependent Mollow triplet of a coherently-driven single quantum dot, Opt. Express **21**, 4382 (2013).

[6] C. Gustin, L. Hanschke, K. Boos, J. R. A. Müller, M. Kremser, J. J. Finley, S. Hughes, and K. Müller, High-resolution spectroscopy of a quantum dot driven bichromatically by two strong coherent fields, Phys. Rev. Res. **3**, 013044 (2021).

[7] O. Astafiev, A. M. Zagoskin, A. Abdumalikov Jr., Y. A. Pashkin, T. Yamamoto, K. Inomata, Y. Nakamura, and J. S. Tsai, Resonance fluorescence of a single artificial atom, Science **327**, 840 (2010).

[8] P. Rodgers and S. Swain, Multi-peaked resonance fluorescence spectra with rectangular laser pulses, Opt. Commun. **81**, 291 (1991).

[9] A. Moelbjerg, P. Kaer, M. Lorke, and J. Mørk, Resonance fluorescence from semiconductor quantum dots: Beyond the Mollow triplet, Phys. Rev. Lett. **108**, 017401 (2012).

[10] K. Konthasinghe, M. Peiris, and A. Muller, Resonant light scattering of a laser frequency comb by a quantum dot, Phys. Rev. A **90**, 023810 (2014).

[11] M. Florjaczyk, K. Rzążewski, and J. Zakrzewski, Resonance scattering of a short laser pulse on a two-level system: Time-dependent approach, Phys. Rev. A **31**, 1558 (1985).

[12] R. Buffa, S. Cavalieri, L. Fini, and M. Matera, Resonance fluorescence of a two-level atom driven by a short laser pulse: Extension to the off-resonance excitation, J. Phys. B: At. Mol. Opt. Phys. **21**, 239 (1988).

[13] K. Boos, S. K. Kim, T. Bracht, F. Sbresny, J. M. Kaspari, M. Cygorek, H. Riedl, F. W. Bopp, W. Rauhaus, C. Calcagno, J. J. Finley, D. E. Reiter, and K. Müller, Signatures of dynamically dressed states, Phys. Rev. Lett. **132**, 053602 (2024).

[14] S. Liu, C. Gustin, H. Liu, X. Li, Y. Yu, H. Ni, Z. Niu, S. Hughes, X. Wang, and J. Liu, Dynamic resonance fluorescence in solid-state cavity quantum electrodynamics, Nat. Phys. **18**, 318 (2024).

[15] V. M. Axt and T. Kuhn, Femtosecond spectroscopy in semiconductors: a key to coherences, correlations and quantum kinetics, Rep. Prog. Phys. **67**, 433 (2004).

[16] J. Danckwerts, K. J. Ahn, J. Förstner, and A. Knorr, Theory of ultrafast nonlinear optics of Coulomb-coupled semiconductor quantum dots: Rabi oscillations and pump-probe spectra, Phys. Rev. B **73**, 165318 (2006).

[17] F. Sotier, T. Thomay, T. Hanke, J. Korger, S. Mahapatra, A. Frey, K. Brunner, R. Bratschitsch, and A. Leitenstorfer, Femtosecond few-fermion dynamics and deterministic single-photon gain in a quantum dot, Nat. Phys. **5**, 352 (2009).

[18] P. Henzler, C. Traum, M. Holtkemper, D. Nabben, M. Erbe, D. E. Reiter, T. Kuhn, S. Mahapatra, K. Brunner, D. V. Seletskiy *et al.*, Femtosecond transfer and manipulation of persistent hot-trion coherence in a single CdSe/ZnSe quantum dot, Phys. Rev. Lett. **126**, 067402 (2021).

[19] M. Zecherle, C. Ruppert, E. C. Clark, G. Abstreiter, J. J. Finley, and M. Betz, Ultrafast few-fermion optoelectronics in a single self-assembled InGaAs/GaAs quantum dot, Phys. Rev. B **82**, 125314 (2010).

[20] T. Suzuki, R. Singh, M. Bayer, A. Ludwig, A. D. Wieck, and S. T. Cundiff, Coherent control of the exciton-biexciton system in an InAs self-assembled quantum dot ensemble, Phys. Rev. Lett. **117**, 157402 (2016).

[21] F. Fras, Q. Mermillod, G. Nogues, C. Hoarau, C. Schneider, M. Kamp, S. Höfling, W. Langbein, and J. Kasprzak, Multiwave coherent control of a solid-state single emitter, Nat. Photon. **10**, 155 (2016).

[22] M. Richter, R. Singh, M. Siemens, and S. T. Cundiff, Deconvolution of optical multidimensional coherent spectra, Sci. Adv. **4**, eaar7697 (2018).

[23] S. Grisard, H. Rose, A. V. Trifonov, R. Reichhardt, D. E. Reiter, M. Reichelt, C. Schneider, M. Kamp, S. Höfling, M. Bayer *et al.*, Multiple Rabi rotations of trions in InGaAs quantum dots observed by photon echo spectroscopy with spatially shaped laser pulses, Phys. Rev. B **106**, 205408 (2022).

[24] C. Ruppert, J. Lohrenz, S. Thunich, and M. Betz, Ultrafast field-resolved semiconductor spectroscopy utilizing quantum interference control of currents, Opt. Lett. **37**, 3879 (2012).

[25] T. Guenther, C. Lienau, T. Elsaesser, M. Glanemann, V. M. Axt, T. Kuhn, S. Eshlaghi, and A. D. Wieck, Coherent nonlinear optical response of single quantum dots studied by ultrafast near-field spectroscopy, Phys. Rev. Lett. **89**, 057401 (2002).

[26] S. Yan, M. T. Seidel, and H.-S. Tan, Perturbed free induction decay in ultrafast mid-IR pump-probe spectroscopy, Chem. Phys. Lett. **517**, 36 (2011).

[27] P. Nuernberger, K. F. Lee, A. Bonvalet, T. Polack, M. H. Vos, A. Alexandrou, and M. Joffre, Suppression of perturbed free-induction decay and noise in experimental ultrafast pump-probe data, Opt. Lett. **34**, 3226 (2009).

[28] R. Mondal, B. Roy, B. Pal, and B. Bansal, How pump-probe differential reflectivity at negative delay yields the perturbed-free-induction-decay: theory of the experiment and its verification, J. Phys.: Condens. Matter **30**, 505902 (2018).

[29] Y. Murotani, M. Takayama, F. Sekiguchi, C. Kim, H. Akiyama, and R. Shimano, Terahertz field-induced ionization and perturbed free induction decay of excitons in bulk GaAs, J. Phys. D: Appl. Phys. **51**, 114001 (2018).

[30] P. Brosseau, H. Seiler, S. Palato, C. Sonnichsen, H. Baker, E. Socie, D. Strandell, and P. Kambhampati, Perturbed free induction decay obscures early time dynamics in two-dimensional electronic spectroscopy: The case of semiconductor nanocrystals, J. Chem. Phys. **158**, 084201 (2023).

[31] P. Hamm, Coherent effects in femtosecond infrared spectroscopy, J. Chem. Phys. **200**, 415 (1995).

[32] L. Seidner, G. Stock, and W. Domcke, Nonperturbative approach to femtosecond spectroscopy: General theory and application to multidimensional nonadiabatic photoisomerization processes, J. Chem. Phys. **103**, 3998 (1995).

[33] C. Wolpert, C. Dicken, P. Atkinson, L. Wang, A. Rastelli, O. G. Schmidt, H. Giessen, and M. Lippitz, Transient reflection: A versatile technique for ultrafast spectroscopy of a single quantum dot in complex environments, Nano Lett. **12**, 453 (2012).

[34] D. E. Reiter, Time-resolved pump-probe signals of a continuously driven quantum dot affected by phonons, Phys. Rev. B **95**, 125308 (2017).

[35] M. R. Klaßen and D. E. Reiter, Optical signals to monitor the dynamics of phonon-modified Rabi oscillations in a quantum dot, Ann. Phys. **533**, 2100086 (2021).

[36] L. Besombes, K. Kheng, L. Marsal, and H. Mariette, Acoustic phonon broadening mechanism in single quantum dot emission, Phys. Rev. B **63**, 155307 (2001).

[37] B. Krummheuer, V. M. Axt, and T. Kuhn, Theory of pure dephasing and the resulting absorption line shape in semiconductor quantum dots, Phys. Rev. B **65**, 195313 (2002).

[38] A. Krügel, V. M. Axt, T. Kuhn, P. Machnikowski, and A. Vagov, The role of acoustic phonons for Rabi oscillations in semiconductor quantum dots, Appl. Phys. B **81**, 897 (2005).

[39] C. Roy and S. Hughes, Polaron master equation theory of the quantum-dot Mollow triplet in a semicon-

ductor cavity-QED system, Phys. Rev. B **85**, 115309 (2012).

[40] M. Cosacchi, M. Cygorek, F. Ungar, A. M. Barth, A. Vagov, and V. M. Axt, Path-integral approach for nonequilibrium multitime correlation functions of open quantum systems coupled to Markovian and non-Markovian environments, Phys. Rev. B **98**, 125302 (2018).

[41] M. Cygorek, M. Cosacchi, A. Vagov, V. M. Axt, B. W. Lovett, J. Keeling, and E. M. Gauger, Simulation of open quantum systems by automated compression of arbitrary environments, Nat. Phys. **18**, 662 (2022).